Distortion of pipe-flow development by boundary layer growth and unconstrained inlet conditions

Cite as: Phys. Fluids **31**, 063602 (2019); https://doi.org/10.1063/1.5091602
Submitted: 04 February 2019 . Accepted: 16 May 2019 . Published Online: 06 June 2019

Herman D. Haustein, and Barak Kashi

Physics of Fluids ARTICLE scitation.org/journal/phf

Distortion of pipe-flow development by boundary layer growth and unconstrained inlet conditions

Cite as: Phys. Fluids 31, 063602 (2019); doi: 10.1063/1.5091602
Submitted: 4 February 2019 • Accepted: 16 May 2019 •
Published Online: 6 June 2019

Herman D. Haustein and Barak Kashi

AFFILIATIONS

Faculty of Engineering, School of Mechanical Engineering, Tel-Aviv University, Ramat-Aviv, 69978 Tel-Aviv, Israel

ABSTRACT

This study extends the analysis of the canonical developing pipe-flow problem to realistic inlet conditions affecting emerging jets. A comparison of simulations to existing theory reveals adverse phenomena caused by the inlet: the velocity profile inversion and flow separation (vena contracta) at a sharp inlet. Beginning with the simple uniform inflow, the inversion is shown to persists at significantly higher Re (Re = 2000) than previously reported. It is found to be caused by the theory's neglected radial velocity, resulting from the boundary layer's displacement effect. Rescaling of the inlet axial coordinate is shown to collapse all centerline velocity curves above Re = 100, thus elucidating the known weak dependence of entrance-length on Re. The sharp-inlet separation bubble is found not to occur below Re ≅ 320 although this inlet profile overrides the boundary layer's effect. Furthermore, the bubble's downstream length increases rapidly with Re, whereas its upstream length grows gradually and proportionally to its thickness—here identified as its characteristic-scale. Beyond the bubble, the profile relaxes to a monotonic form—captured beyond $x/(\mathrm{Re}{\cdot}R) = 0.005$, if theory is modified using the bubble's characteristic-scale. This scale also sets the threshold which differentiates between a sharp-inlet regime, accompanied by a separation bubble, and a rounded-inlet one without it. The latter regime relaxes more rapidly to the monotonic profile—captured already beyond $x = 2R$. Finally, the modified idealized theory is demonstrated as a useful design tool—explicitly relating nozzle length to characteristics of emerging free-surface and submerged jets.

INTRODUCTION

Laminar developing pipe flow has been extensively dealt with, since the early theoretical works of Schiller (1922) and Langhaar (1942). However, it has long been known that even in such a canonical flow, there are strong discrepancies between theory and experiments, both in terms of centerline velocity (Fargie and Martin, 1971), velocity profile shape (Reci *et al.*, 2018), and consequently in nominal entrance/development length [Durst *et al.* (2005), showed that this length varies over $0.052 < X_e < 0.16$ or $0.01 < X_e < 0.015$ for post 1972 data, where $X \equiv x/(\mathrm{Re}{\cdot}R)$]. While these discrepancies may be attributed to differences in inlet conditions or measurement errors, they are seen to persist even in well-established numerical studies with identical inlet conditions. For instance, a recent numerical study by the authors showed that the centerline velocity growth curves only coincide at very high Re or far downstream (Haustein *et al.*, 2017). This is in agreement with the numerical findings of Durst (Durst *et al.*, 2005) that the entrance length is weakly and inversely dependent on the Reynolds number although neither studies provided an explanation for this effect—a matter which is addressed here.

In fact, these discrepancies can be attributed to three primary physical effects: boundary layer displacement, nonuniform inlet velocity profile, and inlet conditions imposed by the transition of the flow into the pipe. An example for the latter was shown in a recent study by the authors (Kashi and Haustein, 2018) where the well-known separation-bubble vortex occurring at a sharp-edged inlet was shown to have significant effect on the velocity profile, an influence that is relaxed beyond $X \cong 0.002$. Understanding these primary physical effects is of crucial importance to many more complex flows, including capillary driven flows, particle laden flows, and turbulent transition near the inlet (Stange *et al.*, 2003; Abbas *et al.*, 2014; Hashmi *et al.*, 2015; and Priymak, 2018, accordingly). Specifically, the occurrence of a flow-separation bubble at the inlet directly affects bubble- and droplet-generating processes based on flow focusing, which has recently received much attention (Mamet *et al.*, 2017). Furthermore, these effects determine the level of issuing profile development, which in turn determines the submerged jet's

interaction with its surroundings during flight (Kashi *et al.*, 2018), impingement heat transfer (Kashi and Haustein, 2018), also with the effect of viscous dissipation at the microscale (Kashi and Haustein, 2019). Similarly, recent works on free-surface jet breakup found a significant influence of the issuing profile—a result of the realistic pipe-flow development (Umemura and Osaka, 2014; Suñol and González-Cinca, 2015).

The development of the velocity profile in channel flow has received much attention over the last century. It was theoretically dealt with early on, for both circular pipes (Schiller, 1922) and parallel plates (Schlichting, 1934), by assuming an idealized uniform-velocity inlet. Later followed by works of Langhaar (1942), Hornbeck (1964), and others, as reviewed and categorized in the work of Fargie and Martin (1971). However, these theoretical studies provided not just complex and often cumbersome solutions, e.g., series-solutions requiring a large number of terms for convergence or iterative solutions imposed by implicit relations [e.g., Sparrow *et al.* (1964)], but failed to differentiate between the end of the potential core (boundary layer meet up) and convergence to fully developed conditions (self-similarly). A later experimental work by Mohanty and Asthana (1979) made this differentiation terming the former the inlet region and the latter the filled region, prior to the fully developed region (see Fig. 1). These observations were approximated at high-Re by a fourth-order Karman-Pohlhausen integral solution for confined flows. By clearly distinguishing between the two regions of flow development, their study was able to address many of the shortcomings of preceding studies, while obtaining good agreement with the experimental measurements. Despite the many simplifications employed, their analysis still required dealing with two coupled nonlinear ordinary differential equations and complex numerical integration, permitting the retrieval of key-flow characteristics, such as the centerline velocity, momentum flux, and shear/vorticity, only in a local/discrete manner. Reviewing the theoretical literature dealing with this problem, several common characteristics are identified of these simplified descriptions: (i) an under-estimation of the radial velocity; (ii) assumption of uniform inflow, which together results in (iii) profiles decaying monotonously from the axis that do not permit off-center peaks, inflection points, or reverse flow to occur. Thereby, key phenomena such as local velocity profile inversion at lower Re and flow focusing or flow separation at the inlet were not addressed, leaving the theoretical solutions to be termed the *idealized description*. Recognizing here as Fargie and Martin (1971) did that "... the entry flow problem is generally regarded as difficult to treat theoretically," a simple approximation is employed in order to obtain a continuous/field description, leading to new insights into the realistic flow and its deviation from this idealized form.

Beyond the required preliminaries, the primary goal of the present study is to shed light on adverse phenomena in realistic pipe-flow development and reconcile previously seen discrepancies. First, the present study considers the dependence on flow rate (Re) of the ideal pipe-flow development (from a uniform inlet), specifically with regards to the occurrence of an off-center peak at the early stages of profile development, sometimes termed profile inversion. This peak was first mentioned by Friedmann *et al.* (1968) and is here attributed to the displacement effect of the boundary layer—whose initial development causes a strong negative radial velocity away from the bounding wall—relatively more prominent for lower axial inertia flows (lower Re). Although contrary to their claims, it does not disappear beyond Re = 500 and is still clearly evident at Re ≥ 1000 in present simulations and recent experiments (Reci *et al.*, 2018). It will be further shown that this off-center peak is the cause for the **lack of self-similarity** in Re of the centerline velocity, previously shown by the authors [Fig. 4(a) in the work of Haustein *et al.* (2017)]. This cause as well as the inlet considerations examined hereafter may well explain the trends of significantly

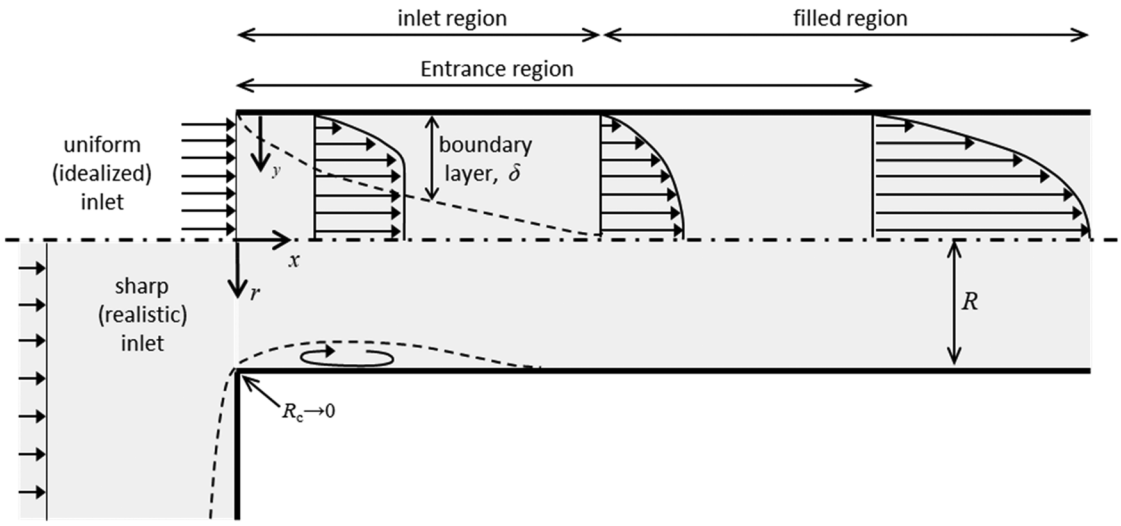

FIG. 1. Schematic of the impinging jet problem, with definition of flow zones.

dispersed experimental data for centerline velocity [Fig. 4 in the work of Fargie and Martin (1971)].

The influence of realistic, nonuniform inlet conditions on pipe flow development is also extensively examined here, especially the occurrence of a separation bubble for high Re, sharp inlet conditions (see Fig. 1). By numerically solving the sharp inlet to a parallel plate channel, Sparrow *et al.* (1964) showed that at higher-Re fluid entering the channel does not conform to it but rather generates a vena-contracta effect—a recirculation bubble at the wall effectively providing the flow with a self-generated rounded inlet. The authors have previously shown that this phenomenon is especially significant in shorter nozzles, where the emerging flow can undergo extra-nozzle acceleration prior to profile relaxation (Kashi and Haustein, 2018). The present study reexamines this phenomenon with the goal of quantifying and bounding its effect—clearly establishing the range of validity of the aforementioned idealized developing pipe flow description. Extending our previous work, the separation bubble is extensively characterized and its scaling with flow rate was identified, as well as the extent of its divergence from the idealized description. It is further seen that its characteristic scale enables extension of the validity range of this description and provides the means to distinguish between the sharp- and rounded-corner flow regimes.

METHODS

In the present work, numerical solutions were employed to obtain the detailed behavior of developing pipe flow in the laminar flow regime and its susceptibility to realistic inlet conditions. In order to show the deviations of this flow from existing idealized theory and for convenient and extensive comparison to it, an approximation is employed based on the simplest previous description—the Karman-Pohlhausen integral solution.

Numerical methods

In the present work, numerical solutions were employed to obtain a detailed view of the velocity and pressure fields of developing pipe flow in the range of Re = 200–2000. Three configurations were studied: (1) a simple pipe with uniform velocity inlet, denoted *uniform* [Fig. 2(a)]; (2) a pipe where the fluid enters from a plenum through an entrance with corner rounding R_c, denoted *round* [Fig. 2(b)]; and (3) similar to the latter, where R_c = 0, is denoted *sharp*.

All pipe models were meshed using quadrilateral cells of uniform size, except three thin layers adjacent to the *wall* boundary. In the *sharp* and *round* model cases, additional cell refinement was added by three successive cell-splitting operations at a region around

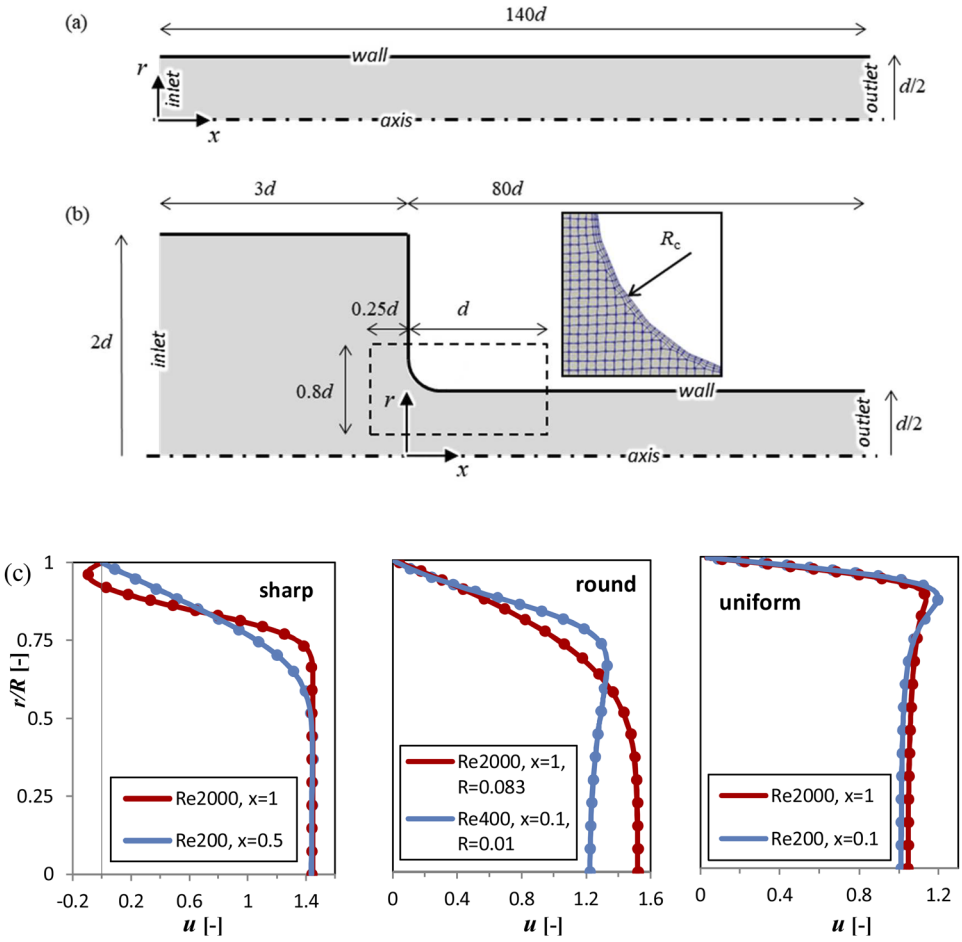

FIG. 2. The geometries of the numerical models with dimensions and boundary names: (a) the uniform case and (b) the *sharp* and *rounded* cases, with the definition of the corner mesh refinement zone, and the inset showing the refined mesh near the corner. (c) Mesh independence tests for all cases. Solid lines—fine mesh. Symbols—coarse mesh.

the pipe entrance corner, as depicted in the inset of Fig. 2(b). The total cell count was 410 760, 324 474, and 314 749 for the *uniform*, *sharp,* and *round* models, respectively. Note that the cell count for the uniform inlet case was highest, in order to enable a very detailed comparison to Mohanty's solution all the way up to fully developed flow, whereas the other two cases required a shorter domain as they focused on the near inlet region.

A uniform velocity profile was imposed at the *inlet* boundary, a no-slip condition at the *wall*, and zero pressure at the *outlet*. The axisymmetric Navier-Stokes equations were then solved using the finite volume open-source computational fluid dynamics (CFD) code OpenFOAM (Greenshields and Weller, 2010), where the velocity and pressure were decoupled using the SIMPLE algorithm with the convergence criteria set to residuals below 10^{-4}. The working fluid was water at 293 K, considered to be Newtonian. Mesh and domain size independence were performed by doubling cell counts and plenum size in the *sharp* and *round* cases, which resulted in negligible effect on the numerical results. The grid was found to be independent of size, as shown for the three different types of inlets considered at the external flow rates in Fig. 2(c). As the figure shows the above-mentioned cell-counts, those corresponding to the "coarse mesh" were more than adequate to capture the flow field accurately.

Beyond validation, these numerical solutions primarily permit examination of different and more realistic inlet conditions, thereby leading to detailed examination of nonidealized flow phenomena.

An approximate description for ideal conditions

The present study also employs an approximation to the idealized pipe-flow development description, based on the Karman-Pohlhausen integral derivation of Mohanty and Asthana (1977; 1979). The present study builds on Mohanty's work, employing their relations for mass and momentum conservation, while breaking the inherent complexity by approximating the centerline velocity evolution and the ratio of the displacement to boundary layer thickness, under strict physical constraints.

In this method, the velocity profile is given by a 4th order polynomial of the form

$$\frac{u(r,x)}{u_c} = 2\eta - 2\eta^3 + \eta^4 + \frac{\lambda_1\left(-\eta^4 + 3\eta^3 - 3\eta^2 + \eta\right)}{6} - \frac{\Gamma_1\left(-9\eta^4 + 20\eta^3 - 13\eta^2 + 2\eta\right)}{2}. \quad (1)$$

Here, the pipe's radial coordinate is converted to the wall-side boundary layer viewpoint by $\eta(r, x) = y/\delta = (1 - r)/\delta(x)$, with $\lambda_1(x)$ and $\Gamma_1(x)$ accounting for the influence of local axial pressure gradient and local velocity profile curvature at the axis, respectively.

Despite the relative simplicity of their method, the analysis by those authors led to two coupled nonlinear ordinary differential equations. These were solved numerically, retrieving δ, λ_1, and Γ_1, presented graphically and sparsely tabulated. In this form, several key flow parameters are only given locally (shear, pressure gradient, momentum flux, etc.) and even the local centerline velocity still required integration over the entire velocity profile. Thereby, their solution does not lend itself to a comprehensive analysis and comparisons, which includes gradients fields and explicit dependencies on pipe-length. For this purpose, the present study approximates elements of the flow in order to deliver a more tractable closed-form, allowing explicit expressions directly applicable to emerging jet flight. By modeling key aspects of the problem, much of the analysis complexity is reduced, avoiding the parameter coupling and the required numerical procedures, while still meeting the physical constraints of mass and momentum conservation, as well as those of self-consistency and physical bounds. This approximation procedure is detailed in the appendix, basically consisting of modeling u_c, then δ, followed by assuming similarity of centerline profile curvature Γ_1 growth to that of the centerline velocity, with λ_1 given by conservation laws, as in the original analysis.

Thereby, it is seen that the new approximation reverses the procedure by Mohanty, whereby the key approximation Eqs. (A1), (A3), and (A8) from the Appendix, close the solution in a simple, explicit manner. The validity of this convenient approximation is demonstrated in the following two figures. A comparison to the somewhat coarse (pitot tube) experimental measurements by Mohanty and Asthana (1977) shows that the present approximation of idealized conditions captures the profile and its development well (Fig. 3).

The new approximation's agreement with previous works dealing with high-Re idealized conditions is quantitatively demonstrated through several key parameters in the next figure. Figure 4(a) compares the centerline velocity development by the new approximation to a large amount of theoretical and numerical solutions. The comparison is intentionally not to experimental results, where additional inlet effects cause deviations from the idealized, uniform-inlet conditions typically considered. This is followed in Fig. 4(b) by an evaluation of the boundary layer growth approximation, again showing

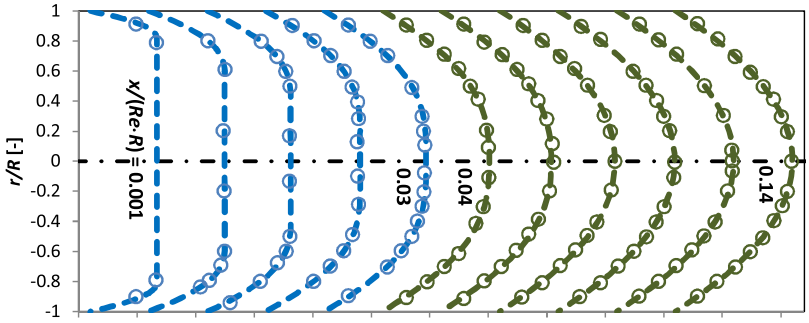

FIG. 3. Axial velocity profile evolution at high-Re (Re ≥ 1875): present approximation vs experimental data (Mohanty and Asthana, 1977).

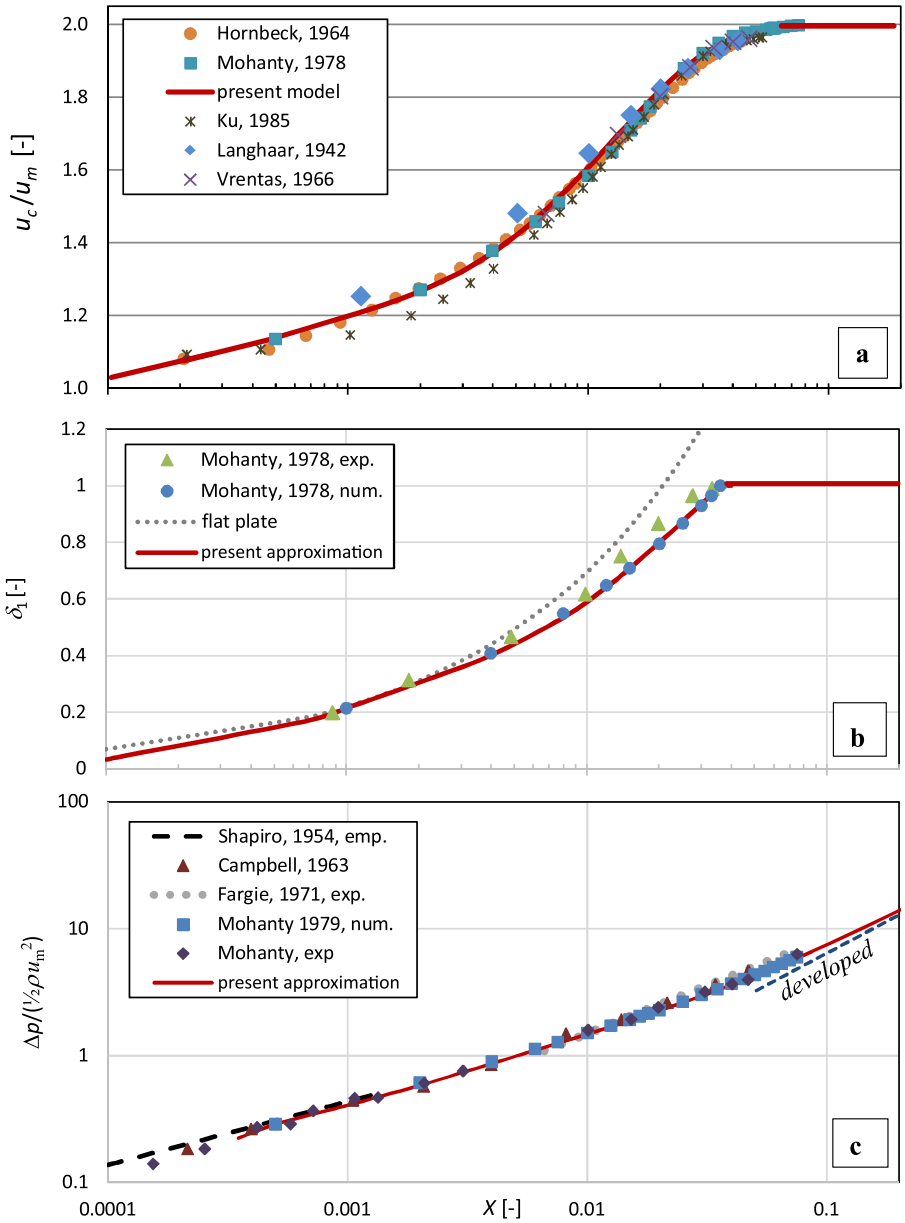

FIG. 4. Evaluation of the approximation through key descriptors: (a) centerline velocity vs previous theoretical and numerical works; (b) boundary layer thickness vs the flat plate solution, Mohanty's solution, and experimental data (Mohanty and Asthana, 1977; 1979); and (c) pressure drop vs previous studies.

good agreement with previous numerical results although somewhat less so with experiments. The figure also shows the gradual divergence from Blasius' flat-plate boundary theory, with departure occurring around the location $\varepsilon = 0.001\,36$ employed in the present approximation. Finally, Fig. 4(c) shows that the pressure drop is not only self-consistent, as was required in the potential core during the development of the new approximation, but that it transitions smoothly from a near-inlet empirical correlation (Shapiro *et al.*, 1954) to the well-known developed Poiseuille pipe flow relation (dashed lines) as well. It is important to note that the pressure drop represents both the flow overcoming the wall-shear and accelerating the core-flow.

Recognizing the validity of the approximation and successful reproduction of the idealized high-Re conditions, it is now used as a reference for examining more realistic conditions and their deviations from ideal flow. Two primary sources of these deviations, which are the often-ignored, are an off-center axial velocity peak and inflow separation at a realistic inlet.

RESULTS AND DISCUSSION

In contrast to the idealized description, realistic boundary layer growth and inflow conditions are shown to cause phenomena which deviated from its monotonous profile, which are not fully relaxed

even by implementing inlet rounding. These phenomena are examined in detail, and their driving mechanisms are identified through reevaluation of the assumptions made in the derivation of idealized description so that they can be related to specific inlet conditions. Modification of these conditions is also examined, leading to a suggested modification of the idealized description—in order to better represent realistic conditions. Finally, some additional advantages of using the proposed approximation are presented, specifically related to the emerging jet characteristics.

The profile inversion phenomenon

Examining the realistic profile distortion phenomenon in order of increasing complexity, simulations in which a *uniform* inlet was still imposed, showed the occurrence of an off-center axial velocity peak—most pronounced at lower Re (see Fig. 5). This peak has previously been experimentally observed and referred to as the profile inversion (Reci *et al.*, 2018)—here clearly identifiable against the ideal description (dotted line). In the last reference, this off-center peak was observed somewhat closer to the pipe axis, possibly due to the practical difficulty of producing a purely uniform inlet profile [see Fig. 4 in the work of Reci *et al.* (2018)]. It is interesting to note that Friedmann *et al.* (1968) claimed that this peak is only relevant to flows below Re = 500 although both present simulations and the experimental observations mentioned found its occurrence at much higher Re.

A comparison to the idealized conditions approximation (dotted line in Fig. 5) reveals that this peak does not quite coincide with the edge of the nominal boundary layer. It is, therefore, hypothesized that it is due to the boundary layer displacement effect—peaking within the boundary layer and that this can be related to the resulting radial flow—generally neglected in the idealized analysis [see discussion in the introduction of the work of Fargie and Martin (1971)]. Therefore, the magnitude of the axial velocity peak is compared to that of the radial velocity taken from the simulations and compared to of the axial peak at several flow rates along the pipe (see Fig. 6). Comparing the first two subplots shows the qualitative similarity between their magnitudes, while the last subplot [Fig. 6(c)] shows that the axial peak's location coincides with that of the local radial velocity. This supports the hypothesis that the radial convection brings excess flow to the boundary layer edge—requiring locally increased axial velocity for compliance with continuity. Understanding that the cause for this peak is related to a *radial* phenomenon, rather than axial one, we proceed to examine its scaling over x/R rather than X. Figure 7(a) shows that the off-center axial velocity peak may reach a magnitude of almost 1.2 times the centerline velocity at around $x/R = 0.2$ for Re = 200, i.e., the peak develops over the first 1/10 of a pipe diameter, decaying from there and becoming unperceivable by $x/R = 10$. In effect, as this is a phenomenon that occurs over a scale of x/R, it is not limited to the low Re range, but requiring an initial development length it emerges only at very low X—a location not easily analyzed at higher Re.

Employing now the scale identified in Fig. 7(a)—where the displacement influence is seen to decay according to an S-curve on a logarithmic scale with a slope of $\sqrt{3}/2$, a new adaptive pipe length scale is proposed

$$X^* = \frac{1+\tanh\left(\sqrt{3/4}\ln(x/R)\right)}{2}\frac{x}{\mathrm{Re}\,R}. \tag{2}$$

Thereby the new coordinate X^* is seen to be a gradual transition to the standard axial coordinate X, whereby the transition function is the complementary of the curve shown in Fig. 7(a), thus taking the correct scaling of the initial displacement effect. Replotting the centerline velocity in this new radial coordinate [Fig. 7(b)] for the entire range of flow rates considered here ($100 \le \mathrm{Re} \le 2000$) shows that all curves collapse to the known ideal high-Re curve already successfully approximated in Fig. 4(a). By contrast, the figure also shows the strongly diverging curve found at lower Re (Re = 100) with the standard scaling in X (double line). However, as Fig. 7(c) shows, while the *centerline* velocities are now all similar, this rescaling is still insufficient for the *full-profile's* distortions. Nonetheless, the wall shear description does seem to benefit from this rescaling, especially near the inlet (beyond the first radius). A better theoretical description, able to take the radial velocity's effect into account over the entire profile, remains to be developed.

To summarize this section, it was shown that the initial off-center peak in the velocity profile scales with the radial velocity caused by the boundary layer growth. The form and rate at which the off-center peak decays in x/R is then employed to modify the initial pipe-flow scaling, leading to a collapse of all flow rate's centerline velocities onto a single curve and better capture of the boundary

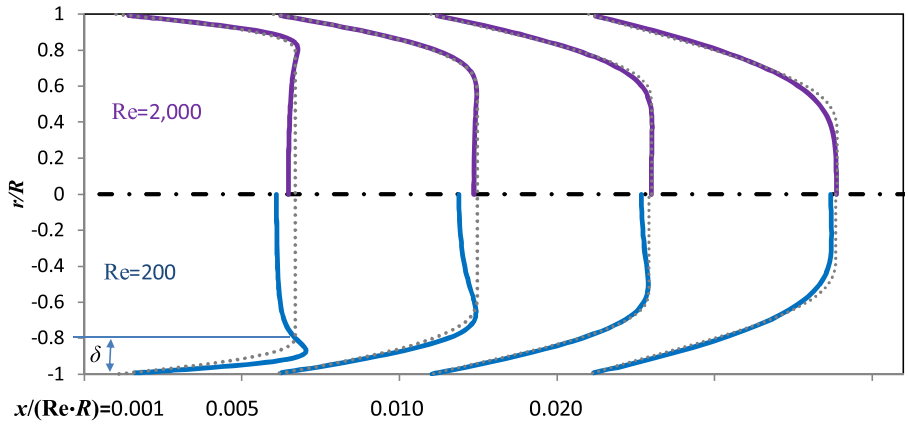

FIG. 5. Simulated profile evolution for a uniform inlet vs idealized description (dotted line). Note that even the high flow rate initially still has an off-center axial velocity peak, while for the lower one, the peak falls within the idealized boundary layer.

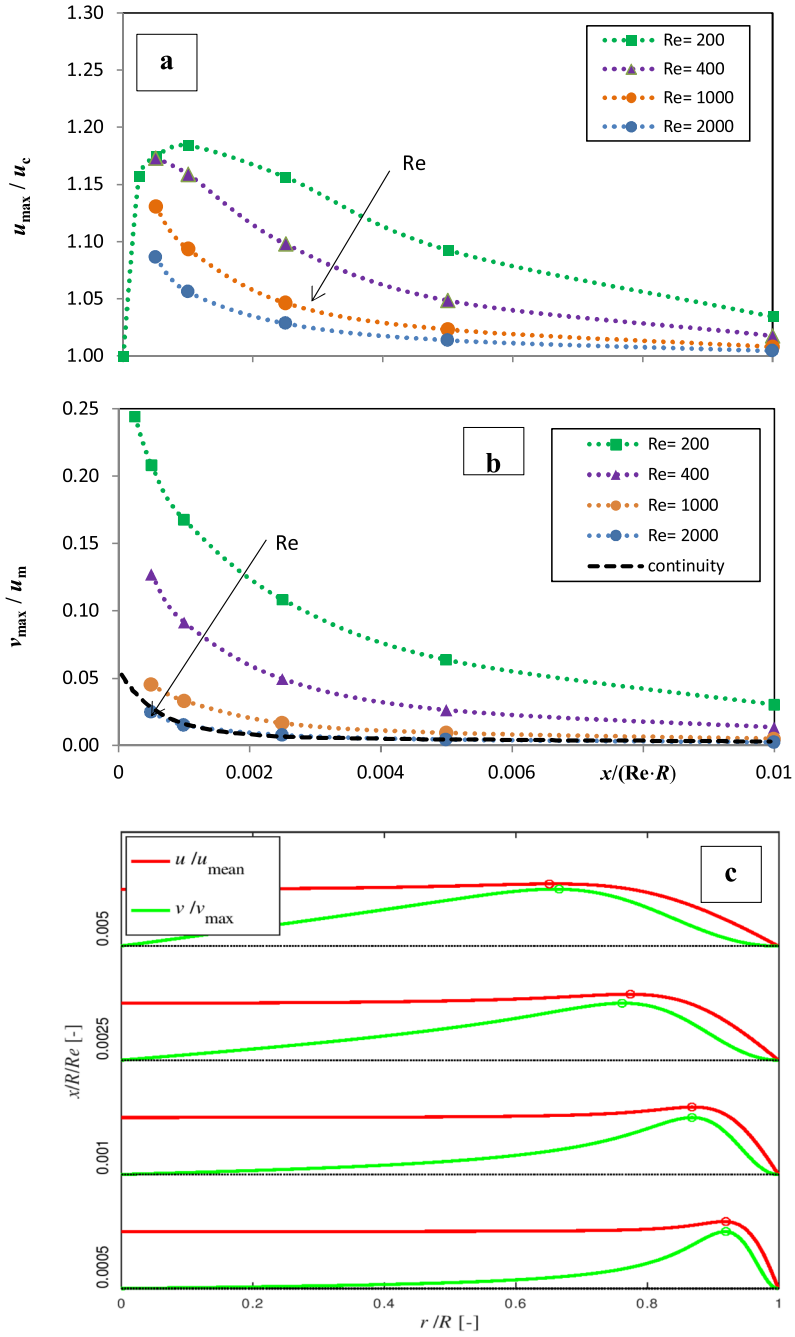

FIG. 6. The relation of radial velocity distribution to the off-center peak in the axial profile: (a) the magnitude evolution of the peak at several flow rates; (b) maximal radial velocity evolution at several flow rates; and (c) detailed axial vs radial velocity profiles at a low flow rate (Re = 200).

layer velocity gradients. With the isolation of this inherent displacement effect, we now turn to address the additional flow-focusing inlet effect.

The inlet separation bubble phenomenon

Beyond a uniform inflow, a more realistic *sharp inlet* is known to cause a "vena-contracta" phenomenon at higher Re. Following the previous insights, the inlet region, and specifically the vena-contracta's separation bubble occurring there at higher Re, is examined in x/R terms. The details of the separation bubble's geometry are given in Fig. 8(a), differentiating its upstream length—from the inlet to its thickest point, its downstream length—from there up to the point of reattachment, and its maximal thickness. These parameters normalized by the radius are plotted against flow rate in Fig. 8(b). Closer examination revealed that below Re = 300, the bubble does not occur, and an effort to pin-point it led to a

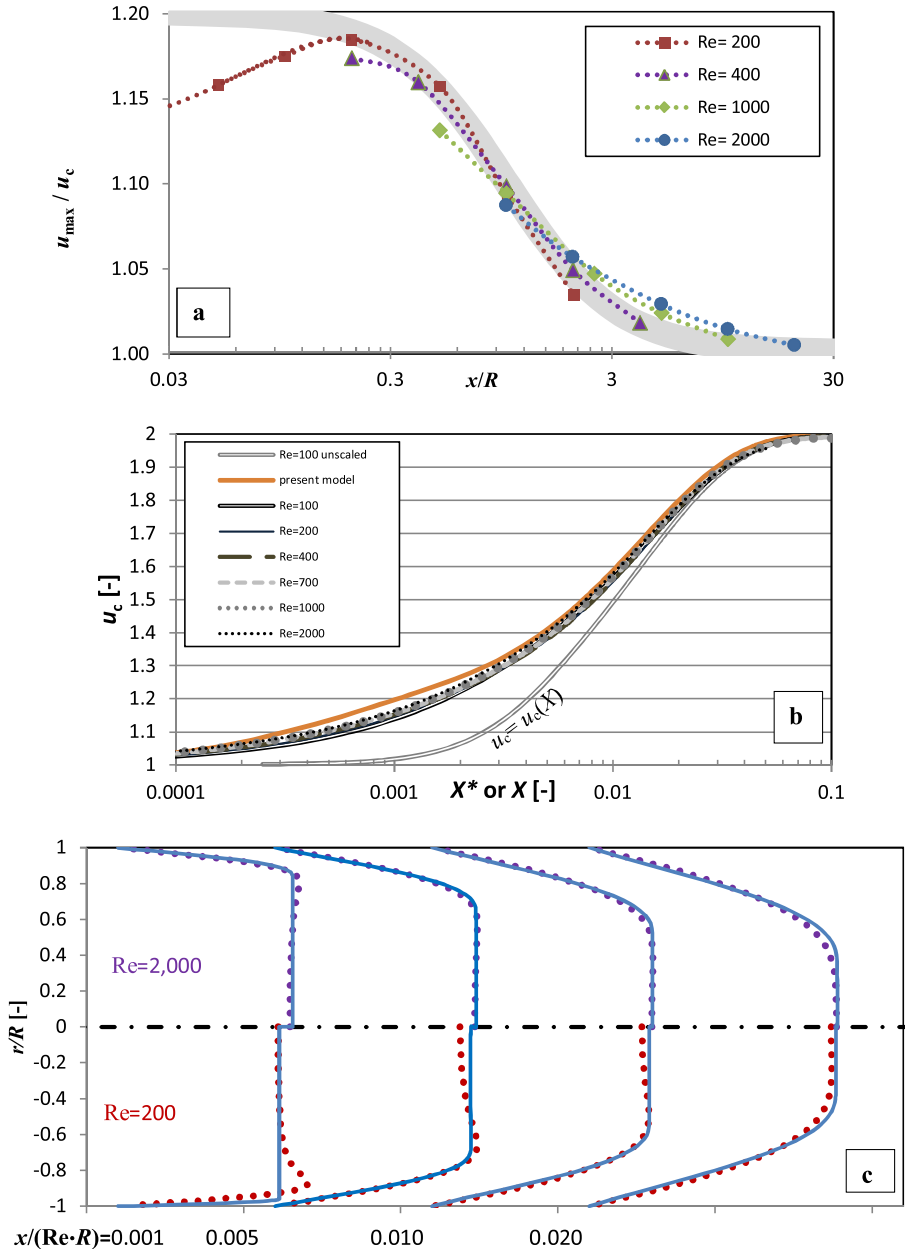

FIG. 7. The new axial rescaling of the inlet region: (a) off-center peak magnitude decay; (b) centerline velocity collapse to a single curve by employing X^*; and (c) improved profile capture by employing X^*.

cut-off value at Re = 320. On the other hand, at higher Re, the figure shows that the downstream length becomes significantly higher than the upstream value. Most importantly, it is shown that the upstream length and bubble thickness scale similarly with flow rate (Re) with a ratio of about ~4.5 between them.

Following a previous study by the authors Kashi and Haustein (2018), which showed that the inlet separation bubble sped-up the pipe flow development, an effective-length modification to the idealized description is sought. The addition of this equivalent inlet length accounts for the displacement by the bubble and resulting rapid centerline acceleration. Therein, the present study first delimits and then extends the validity range of the idealized description by employing an equivalent inlet length (similar to a virtual-origin modification used in jet-flows; Watson, 1964; Revuelta *et al.*, 2002; and Kashi *et al.*, 2018; Andrade and Tsien, 1937; and Schwarz and Caswell, 1961.

Examining the upstream bubble length (or thickness) as the characteristic scale for this type of inlet, it is seen to have a power-law dependence on flow rate at higher-Re (Re ≥ 1000) as

$$L_u \sim \mathrm{Re}^{5/8} \Rightarrow \Delta X = C\mathrm{Re}^{-3/8} \cong \frac{1}{16}\mathrm{Re}^{-3/8}. \quad (3)$$

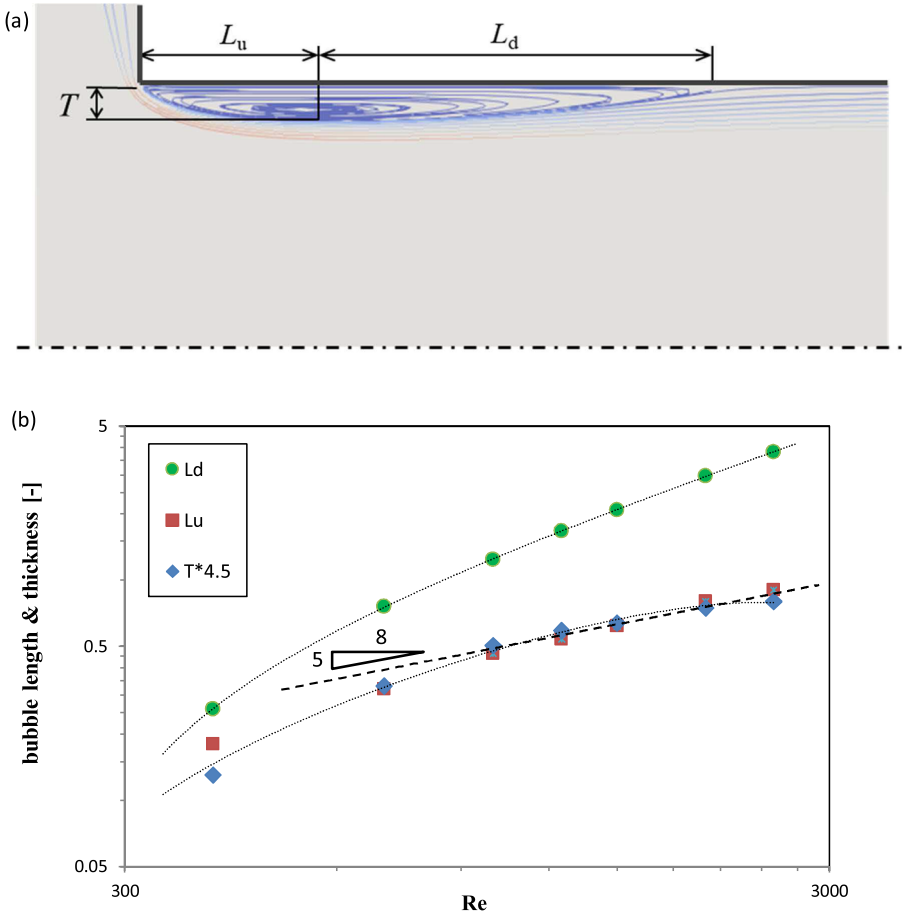

FIG. 8. The sharp-inlet separation bubble characteristics: (a) streamlines colored by velocity magnitude at Re = 2000 and showing separation bubble form and (b) summary of the bubble size dependence on flow rate—no bubble could be found below Re = 320.

Moreover, understanding that this separation bubble completely diverges the boundary layer growth from the idealized description [see Fig. 4(b)], it is seen to override the previously examined displacement effect. In other words, instead of the displacement rescaling X^*, beyond the separation bubble, the traditional pipe flow scaling X is quickly recovered although with an offset. Therefore, an equivalent inlet length ΔX is sought, which will account for the influence of the initial separation bubble in traditional scaling terms X. Taking the inlet bubble as a guide for finding this equivalent length and noting its scaling with flow rate ($\sim Re^{5/8}$) led to the form suggested in Eq. (3). Whereby, with the most suitable value for the constant, found by comparison to a range of simulations, is around 1/16.

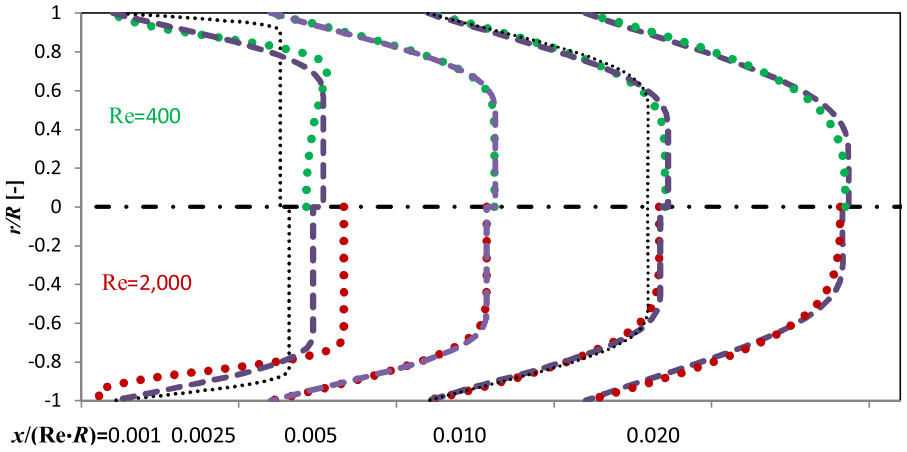

FIG. 9. Developing velocity profiles for a sharp inlet at two flow rates: simulated (dots), idealized description employing X^* (dotted line), and idealized description employing ΔX (dashed lines). Note reverse flow near the wall at X = 0.001 and Re = 2000.

This constant's value is in agreement with previous observations by the authors that the inlet bubble generates an effect equivalent to an inlet length of around $X = 0.0035$ at high-Re (Kashi and Haustein, 2018).

The modification of the ideal pipe-flow description by this equivalent inlet length is seen to be able to account for the sharp inlet effect and its dependence on flow rate starting at $X \cong 0.005$, as demonstrated in Fig. 9. For comparison, the previous displacement-dominated initial profiles (dotted lines) are shown to be unable to account for the inlet separation-bubble's effect. While this modification to idealized theory may seem sufficient, at high-Re, this value is equivalent to many radii. Alternatively, pipe inlet rounding is often encountered, whether as a means to prevent inlet flow separation or just due to practical manufacturing limitations, especially at the microscale.

The inlet separation bubble elimination

Although typically inlet rounding is addressed in an engineering fashion, here a different approach is taken—examining whether the flow can dictate the required level of rounding for rapid inlet-disturbance relaxation. In other words, it is suggested that the separation bubble's characteristics give the sufficient measure of inlet rounding in order to eliminate the bubble's occurrence and give smooth and rapid convergence to idealized developing pipe flow. However, there remains the question of whether the smallest scale—the bubble thickness or the upstream bubble length are its characteristic scale, which dictates the required rounding. This matter was hereby resolved through a series of simulations conducted at several flow rates (Re = 400–2000). This parametric study (not shown) ranging from a rounding of 1/5th of T and up to $4.5T$ ($\cong L_u$) revealed that indeed an inlet rounding with a radius equal to the bubble thickness (T) is the minimal rounding for rapid flow relaxation. This is demonstrated in Fig. 10(a) by employing this scale for two extreme flow rates, previously shown to have a distinct inlet separation bubble. As can be seen from the profiles shown in the figure, not only is the separation bubble now eliminated (no reverse flow near the wall), but employing the previously found equivalent inlet length also in this case, permits capture of the resulting profiles much nearer the inlet – already from around $x = 2R$ at high-Re and even sooner at lower Re. The suitability of the sharp corner equivalent inlet length for this case too demonstrates how using the bubble thickness as the measure for inlet rounding has maintained the similarity between these two problems, while the rounded inlet has the advantage of more rapid recovery from the inlet distortions. Figure 10(b) summarizes the remaining gap and unaccountable deviations from the idealized description, even when employing the suggested axial coordinate modification. As the figure

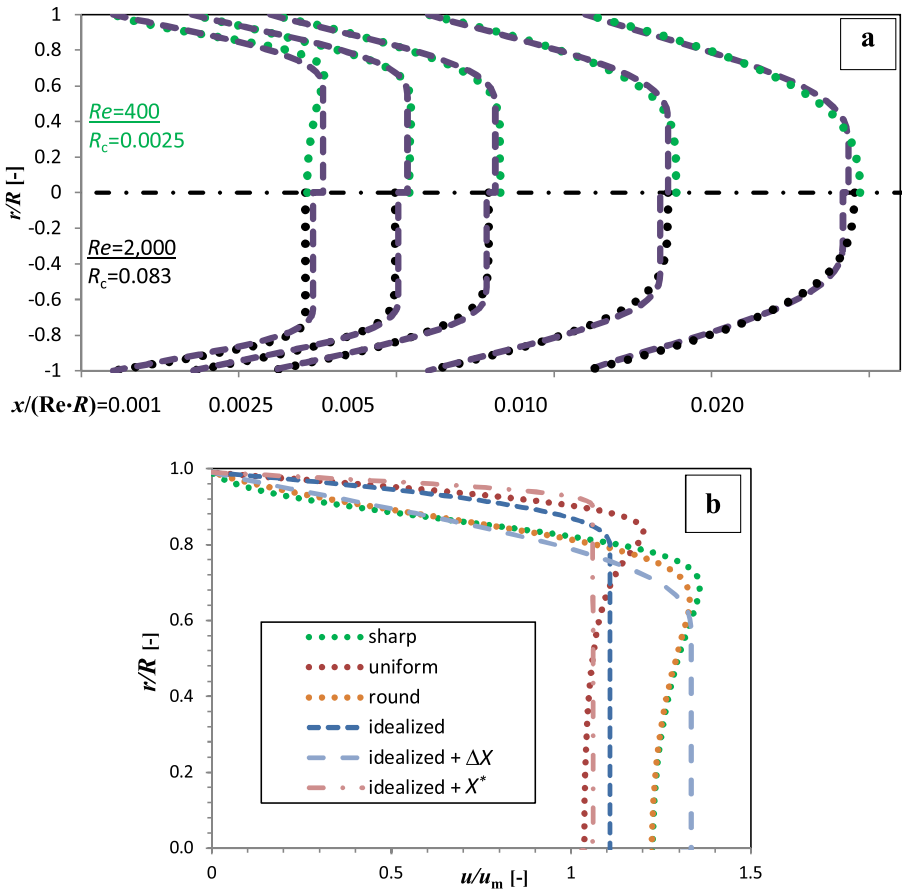

FIG. 10. Developing velocity profiles summary: (a) a rounded inlet at two flow rates vs the idealized description employing ΔX (dashed lines) and (b) a comparison of all cases near the inlet ($x = 0.4R$, Re = 400) vs corresponding modified idealized description (dashed lines).

shows, at a typical low-Re of 400, no two inlet-conditions generate the same profile within the first pipe-diameter. The closest profiles are that of the sharp corner and minimal rounding inlets although as may be expected that the rounded one is more relaxed. Therein, the suggested axial coordinate modification for each case follows the trends very well although does not yet capture the centerline velocity and wall shear value very well. It eventually converges to the real profile farther downstream—beyond the first pipe diameter. The present study, by characterizing the phenomena and identifying their scaling, lays the foundation for further development of theory for realistic conditions, especially for this near inlet region.

Use of the approximation for jets

Up to this point, the approximate idealized description has been employed for convenience and reference only to clearly establish the distortions of realistic developing pipe flow. Considering it now as a predictive tool, it is seen that its modification by rescaling the inlet or employing an equivalent inlet length can account for the distortion caused by various types of inlets. As the study is motivated by the study of jets emerging from short, pipe-type nozzles, it is now examined whether this approximation contributes to the understanding of their characteristics. A key influence on jet flight is the emerging momentum flux [sometimes referred to as the jet thrust (Davies *et al.*, 1977)]. Previous studies, including those by the authors, have elucidated it importance: For a horizontal free-surface jet, it directly dictates the level of jet contraction (Haustein *et al.*, 2017), while for submerged jets, it dictates the potential- and boundary-core lengths (Kashi *et al.*, 2018). First, the increase in momentum flux during pipe flow development is seen to be well captured by the present approximation although a comparison to past and present numerical results, followed by its application to jet flight.

The dimensionless momentum flux is defined as

$$M_p(x) = \frac{2\pi}{\pi R^2 \cdot u_m^2} \int_o^R u^2(x,r) \cdot r dr, \tag{4}$$

where u is given by Eq. (A1) subject to all the elements given in Eqs. (A2)–(A9). While the full expression for the velocity distribution is too large to show here, the approximation is explicit and analytical integration can be performed to obtain the momentum flux. More importantly, asymptotic analysis can be conducted for the large resulting expression. Approaching developed conditions, the expression at leading order is much simpler and the **upper asymptote** can be written as

$$\lim_{X\to\infty} M = \frac{4}{3} - \frac{17e^{-36X}}{49} + \frac{e^{-36(X-0.036)}}{21}. \tag{5}$$

For constant curvature profiles (such as the uniform and fully developed extremes), the momentum-flux can be expressed through the centerline velocity. However, it is clear that during the development process, the outer regions ($r \to ½$) will have higher curvature and consequently higher momentum flux, and the centerline expression is a **lower bound**. Requiring its conformance to the well-known inlet and developed momentum flux values, $1 \le M \le 4/3$, gives

$$M \ge \underbrace{\left(2 - \frac{2}{13}e^{-1150X} - \frac{11}{13}e^{-36X}\right)}_{u_c}^{\frac{\ln(4/3)}{\ln(2)}}. \tag{6}$$

Figure 11 shows the full approximation (dotted line) and its good agreement with present simulations and a previous extensive numerical analysis (Gavis and Modan, 1967). It is important to note that the original curve by Gavis required significant numerical effort, whereas the closed-form approximation developed here, although somewhat lengthy, is explicit and continuous and may easily be employed in an optimization procedure. Note that the upper asymptote [Eq. (5)] holds already from around $X = 0.015$ and covers the majority of the developing flow, while the lower bound trails by $\Delta M \cong 0.04$ over most of the range. For a simple expression for the momentum flux covering a wider range, the harmonic mean of these two limiting expressions can be taken (solid curve). This mean is seen to be a very good approximation to the simulated results already from $X \ge 0.003$—the range of validity of the idealized

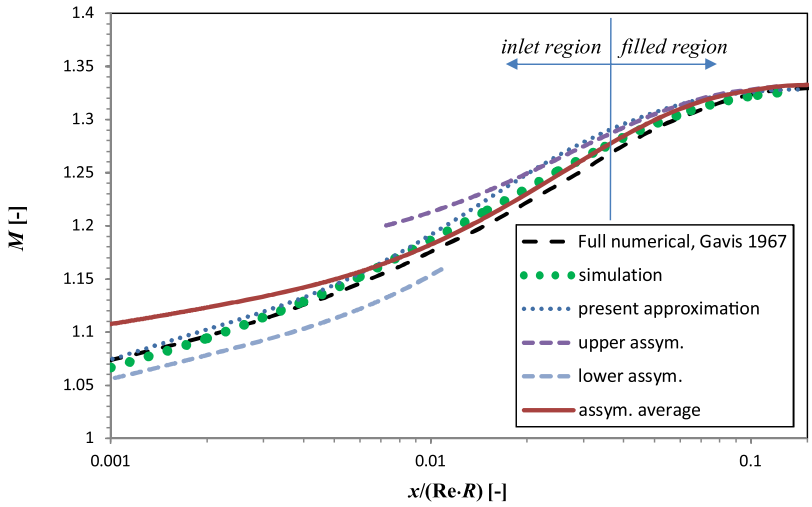

FIG. 11. Dimensionless momentum flux: present approximation vs present simulations and previous theory, showing new asymptotes for $X \to 0$, $X \to \infty$, and their harmonic mean.

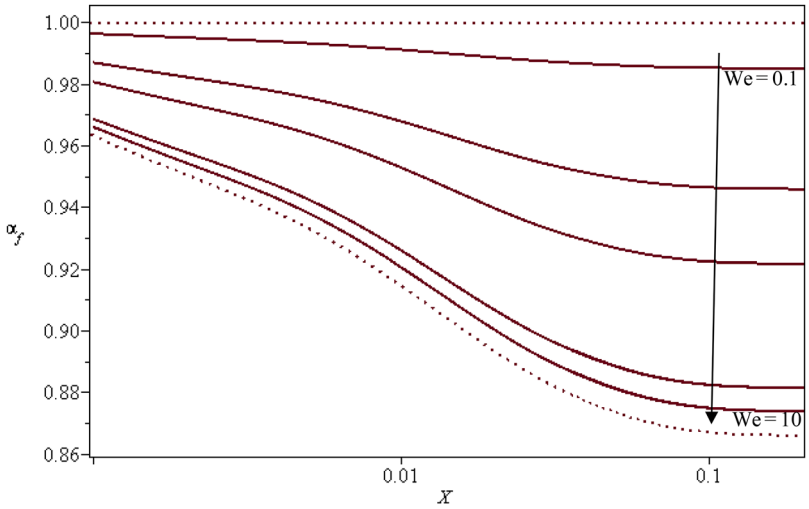

FIG. 12. The final contraction level of a free-surface jet and its explicit dependence on nozzle length and liquid-gas surface tension (We = 0.1, 0.5, 1, 5, 10), dotted lines indicate possible range.

description identified above, while still requiring minimal calculation effort. Some more advantages of the new approximation for the description of jets are demonstrated in Figs. 12–14.

Employing the full approximation for the momentum flux, it is possible to present several key parameters of jet flight in a new way. Figure 12 shows a free-surface jet and its final level of contraction, converged during inflight relaxation. The figure was derived by introducing the full approximation of $M(X)$ into the contraction level's explicit solution [Eqs. (12)–(15) in the work of Haustein *et al.* (2017)]—a solution to the integral momentum conservation relation, first derived by Gavis and Modan (1967) as

$$0 = \frac{2}{\mathrm{We}}\alpha_f^3 + \left(M - \frac{2}{\mathrm{We}}\right)\cdot\alpha_f^2 + 1, \tag{7}$$

where α_f is the final level of horizontal jet contraction. This figure shows a new form of representation—tying the level of contraction directly to pipe length, instead of through the corresponding derived issuing momentum flux [the latter already shown in the Haustein *et al.* (2017)]. Such an explicit dependence is crucial for the free-surface jet design, tying the local momentum flux to a known geometric parameter (pipe length) for the first time, and avoiding the complexity of deriving it from classical pipe-flow studies—where it is typically not shown.

Similarly, for submerged jets, it is now possible to represent two key flow characteristics and their explicit dependence on nozzle length—the potential core and boundary core for jet flight (see Fig. 13). The former is quite well-known and depicts the domain which has not yet lost its initial issuing velocity, whereas the latter may be even more significant and has only recently been clearly identified by the authors (Kashi *et al.*, 2018). By recognizing that highly developed profiles will undergo internal relaxation long before being influenced by the ambient conditions transmitted by diffusion (e.g., shear, but not pressure), rather than taking the magnitude of the velocity relative to its initial value, the boundary core

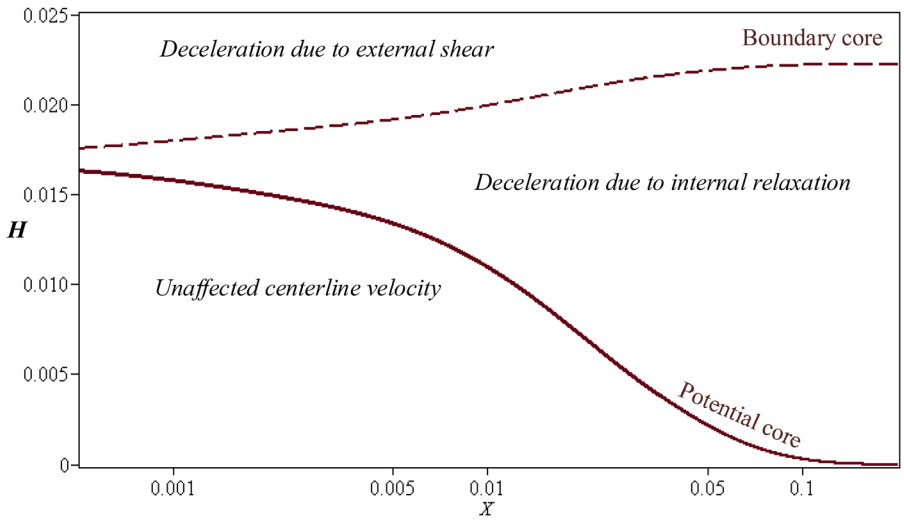

FIG. 13. The potential core and boundary core lengths of a submerged jet and their explicit dependence on the nozzle length, delimiting the domains of influence.

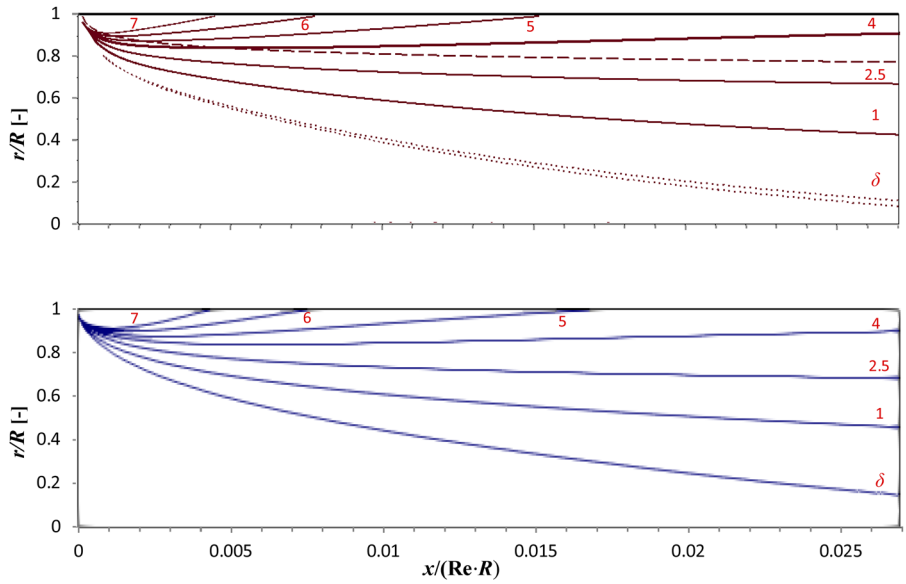

FIG. 14. Approximate iso-shear lines (top) vs simulation (bottom). Note that the dashed line indicates maximal shear penetration, the double dotted line is the boundary layer edge, and numerals indicate dimensionless shear magnitude, $\tau/(\frac{1}{2}\rho u_m^2)$.

traces the boundary condition's diffusive penetration into the jet. Thereby demonstrating that the potential core alone is an insufficient descriptor and resolving a key issue—while a fully developed profile **does not** have a potential core, the boundary condition's penetration into the core of the jet still takes a **finite** distance (or amount of time)—given by the boundary core. Thereby it defines the domain still unaffected by the surroundings, while permitting internal relaxation to occur—a concept easily translatable from momentum to heat and mass transfer as well. The domains of influence on the centerline velocity are clearly mapped out in geometric parameters in Fig. 13.

Beyond the convenience of the present continuous approximation, it also assists in examination of the shear field of the developing flow, shown in Fig. 14. As the figure shows, not only is the present approximation in good agreement with the simulations, but interesting aspects of the shear are easily found—such as the maximum penetration of a given shear level into the flow (depicted by the dashed line) or the trace of the developed flow wall-shear (bold line). The *near-wall* emerging shear level is of primary significance to the initial widening of a submerged jet [see Fig. 15 in the work of Kashi *et al.* (2018). Initial jet-widening based on a finite velocity criterion is dependent both on the initial shear with the surroundings and on the relaxation of the emerging profile—i.e., on the gradients somewhat more interior than the jet edge. The radial location at which the shear is representative of the initial jet-widening can be found although depends on the chosen criterion for jet-width. By providing the entire idealized shear field (see Fig. 14), the present study enables convenient jet-widening analysis given a particular criterion, within the validity range of this description. This analysis goes beyond the scope of the present study and is left for future research.

CONCLUSIONS

The primary contribution of this study is the insight gained into the two different causes for velocity profile distortion and delayed convergence to the nominal monotonic idealized profile. Therein, the present study deals in detail with boundary layer displacement flow and flow entrance into the pipe, as well as their effects on the initial profile and the relaxation thereof. First, it was identified that all previous theoretical works were based on an idealized description of pipe flow development—characterized by neglected radial velocity, monotonous profiles, and uniform inflow. Next, each of the idealized description's assumptions was released, in turn, and the resulting realistic deviations were characterized and analyzed. In general, these deviations may well explain the wide dispersion of results shown in the literature review.

First, maintaining the uniform inflow assumption and examining low Re flows, the well-known off-center peak in axial velocity was found through numerical simulations. Moreover, comparing the idealized description to laminar high Re flows revealed that despite its reduction this peak persists up to Re = 2000—the highest value reported to date. Considering continuity, the negative radial velocity due to boundary layer displacement was closely examined and seen to correlate strongly with the location and magnitude of this peak. Subsequently, it was found that the peak magnitude scales with x/R rather than the typical scale $x/(\mathrm{Re}\cdot R)$. This led to suggesting a new adaptive streamwise scale transitioning from one to the other (X^*), which now collapses the centerline velocity growth curves for all laminar flows above Re = 100, previously shown to coincide only at very high-Re (Haustein *et al.*, 2017). The downstream trace of this initial divergent scaling also explains the weak Re-dependence of the development length, thereby resolving this departure from self-similarity identified in a recent review (Durst *et al.*, 2005).

Next, a more realistic sharp-corner inlet is considered and seen to generate the well-known vena contracta phenomenon and associated inlet separation bubble, which is here characterized in detail. Closer examination revealed that this bubble does not occur below Re ≅ 320 although the inlet profile is still distorted, thereby overriding the simple boundary layer and its aforementioned effect. So much so, that it relaxes back to the idealized form only beyond

$x/(R\cdot\mathrm{Re}) = 0.02$—equivalent to $40R$ at Re = 2000. In addition, it was found that while the downstream bubble length increases rapidly with Re, its upstream length grows more gradually and proportionally to the bubble thickness—i.e., the upstream side grows isotropically with flow rate. It is further shown that taking the latter as the bubble's characteristic scale and rounding the inlet edge according to it eliminates the flow separation although significant profile distortion still exists. Thereby a new physical, quantitative threshold for regime transition is hereby identified, clearly distinguishing a "sharp" corner flow regime with a separation bubble and a "rounded" corner one without separation. These findings are of great importance to future studies on transition to turbulence, particle laden flows, and especially for high-Re flow-focusing configurations.

In this study, a closed-form, continuous approximation was employed for the idealized description, which still adheres to conservation laws, in order to identify the deviations of realistic flows from it. Modification of the idealized description is suggested, in terms of axial coordinate rescaling or the use of an equivalent inlet length able to partially account for the distortion of the initial profile due to inlet effects. This modification extends the validity range, enabling the idealized description to capture the sharp corner inlet flow from $x/(\mathrm{Re}\cdot R) = 0.005$ and rounded corner already by $2R$ and providing a readily useable description of developing pipe flow, for design and optimization purposes.

Finally, this approximation is seen to directly provide the dependence of momentum flux on pipe length—a key parameter for the flight characteristics of an emerging free-surface or submerged jet—elementary flow configurations with numerous applications. The present study maps out in geometrical terms the domains of influence on the submerged jet centerline, for the first time, clearly identifying when the jet core becomes subject to external diffusive influences. Beyond this fundamental insight, the new analysis also enables better design of both free-surface and submerged jets and can directly be employed in an optimization scheme. Finally, it has laid a foundation for describing the initial submerged jet widening upon emergence from a pipe-type nozzle, relevant to jet-surroundings interaction, and optimal jet-to-jet spacing in an array, the details of which remain to be undertaken in a future study.

ACKNOWLEDGMENTS

The authors would like to acknowledge the funding support from the Israel Science Foundation, Grant No. 4112/17.

APPENDIX: SIMPLE PIPE FLOW APPROXIMATION

Proceeding in a reverse order of Mohanty's analysis, we first model its final, rather complex, stage and find that the centerline velocity, then working back through the boundary layer shape, yields the remaining unknowns (λ_1, Γ_1) while maintaining conservation laws. In the light of previous analysis of momentum diffusion processes in cylindrical jets (Duda and Vrentas, 1967; Haustein *et al.*, 2017; and Kashi *et al.*, 2018), it is proposed that the centerline velocity increase, during flow development, can be approximated by an exponential series. Thereby these previous analyses were purely of convection-diffusion cases, whereas here the local pressure gradient is not overlooked, but rather approximated by a locally dominant exponential rate of change. For simplicity, the lowest order representation of this exponential series is employed, which includes only two terms—representing the *early* and *late* stages of flow development

$$\frac{u_c}{u_m} = 2 - f\cdot\exp(-\gamma_1 X) - (1-f)\cdot\exp(-\gamma_2 X), \tag{A1}$$

where it is understood that the initial velocity growth rate is much larger than the later rate ($\gamma_1 \gg \gamma_2$), while f is a weighting fraction—controlling the transition from the dominance of one to the other while satisfying the inlet and fully developed conditions. The rate of initial growth will be found through the subsequent analysis, while the rate of later growth has previously been shown to have the value $\gamma_2 = 39$ (Haustein *et al.*, 2017) in order to meet the well-known development length requirement, $u_c = 0.99$ and $u_{c,f} = 1.98$ at $X_e \cong 0.1$ (Incropera *et al.*, 2011). Later works have suggested somewhat higher values of $X_e \cong 0.11$ [see review in the work of Durst *et al.* (2005)]—equivalent to $\gamma_2 = 36$, the value used here. Note that due to the driving pressure this value must be somewhat above the relaxation rate of an emerging jet, found analytically by Bohr's to be $\gamma_1 = 29.37$ (Bohr, 1910).

Following Mohanty, the thin shell-approximation is employed, giving the boundary layer displacement thickness from continuity through

$$\frac{u_m}{u_c} = 1 - 2\frac{\delta_1}{R}. \tag{A2}$$

Up to this point, the analysis (last two equations) is common to both regions of flow development (see Fig. 1) although in the following each region is dealt with separately, then closing the analysis in a joint description.

1. Inlet region

Due to the accelerating potential core flow in the inlet region, the boundary layer velocity profile transitions from one similar to that of a flat plate to a much more curved one, characterized by a lower displacement thickness (such as seen in Falkner-Skan type accelerating flows). As the flat plate boundary layer is known to grow according to a power-law relation, an approximation of the same sort is employed for the evolution of the ratio between the displacement and boundary layer thickness within the inlet region

$$\frac{1}{\Delta} \equiv \frac{\delta}{\delta_1} \Rightarrow \frac{\Delta_i/\Delta - 1}{\Delta_i/\Delta_f - 1} = \left(\frac{X}{X_f}\right)^n, \tag{A3}$$

where $\Delta < 1$ is the displacement to the boundary layer thickness ratio, with a value of $\Delta_i = 3/10$ given by Mohanty's solution at $X = 0$ for the accelerating flow (slightly below Blasius' flat plate value of 0.344). On the other hand, at the end of the inlet region ($X_f = 0.036$), $\delta = 1$ and $\delta_{1,f} = \Delta_f \cong 0.218$ can be derived from Mohanty's tabulated velocity ($u_c = 1.774$) through Eq. (A2). Thus, leaving only the power n to be found from physical considerations.

As will soon be shown the solution in both the inlet and filled region contains no additional model parameters beyond f, γ_1, and n, which can be uniquely found from physical and consistency constraints. First, it is understood that at no point may the *accelerating* pipe-flow boundary layer grow above that of a flat plate subject to the same inlet velocity. More significantly, near the inlet both boundary

layers will grow at the same rate, prior to a non-negligible rise in the core velocity. Therefore, the limit near the inlet is given by

$$\frac{d\delta}{dx} \xrightarrow{x\ll 1} \frac{d\delta_{fp}}{dx}. \tag{A4}$$

Moreover, as both boundary layers begin at zero near the inlet, they should be equal in magnitude as well

$$\underbrace{\frac{1}{2}\left(\frac{u_c-1}{u_c}\right)\left(\frac{1}{\Delta_i}+\left(\frac{1}{\Delta_f}-\frac{1}{\Delta_i}\right)\left(\frac{X}{X_f}\right)^n\right)}_{\delta}\Bigg|_{0<X=\varepsilon\ll 1} = \underbrace{4.9\sqrt{2}X^{1/2}}_{\delta_{fp}}\Bigg|_{0<X=\varepsilon\ll 1}. \tag{A5}$$

Here, the RHS of the equation is the well-known Blasius solution for flat plate boundary layer thickness, whereas on the LHS is the pipe inlet boundary layer expressed in terms of u_c by substituting Eq. (A2) into Eq. (A3) and rearranging.

We now seek a proper value for ε at which to apply these new constraints. Comparing Mohanty's results (their Table 1 and Fig. 4) to the Blasius solution shows the pipe-flow boundary layer begins to fall below that of the flat plate around $\varepsilon \cong 0.0015$. It is well known that Blasius' solution [RHS of Eq. (A5)] only becomes valid beyond an initial distance over which self-similarity is obtained. Comparing to second-order boundary layer descriptions, it is seen that the first-order (Blasius) solution becomes valid around $\mathrm{Re}_x = 1000 = X\,\mathrm{Re}_d^2$ [see Schlichting (1967), Fig. 7.11]. This value together with a characteristic value for the laminar range of pipe flow ($\mathrm{Re}_d^* = \sqrt{320}\cdot\sqrt{2300} \cong 860$)—the geometric mean of the identified self-similar flow range [see Fig. 8(b)]—leads to required agreement at $\varepsilon \cong 0.001\,36$. Introducing this location into Eqs. (A4) and (A5) together with the boundary meetup location $X_f = 0.036$ and requiring the equality there of both value and derivative dictates the first two relations between n, γ_1 and f—the latter two parameters contained within u_c according to Eq. (A1).

The last constraint is given by the requirement of self-consistency of the model in pressure terms. On the one hand, introducing Eqs. (A1) and (A3) into Mohanty's analysis gives the pressure distribution within the pipe (as detailed below), which is then required to agree with the introduction of Eq. (A1) into the inviscid Bernoulli relation within the pipe core, $\Delta p = u_c^2 - 1$. In other words, following the analysis of Mohanty although with present approximations for its simple closure gives the pressure drop's dependence on X. By simultaneously requiring that this dependence agrees with Bernoulli's relation provides the last missing constraint. This third constraint limits model parameters even further, and it is claimed that as there are three approximation constants and three physical constraints, thereby resulting in effectively no *fitting* parameters. The first two constraints are rather straightforward, whereas the last requires an iterative search detailed in the next paragraph, resulting in a set of constants: $\gamma_1 = 1150$, $f = 2/13$, and $n = 0.43$. These are coupled through the defined constraints, which are strictly met, as shown in Fig. 15. This set leads to an initial pressure drop within the pipe ($X < 0.002$) of $\Delta p \propto X^{0.51}$ which compares very well with the empirical relation of the work of Shapiro *et al.* (1954) which claims $\Delta p \propto X^{0.5}$.

The pressure drop consistency requirement employs the following relations, given in Mohanty's solution:
Within the inlet the dimensionless pressure gradient is given by

$$\lambda \equiv \frac{\delta^2}{\mu u_c}\frac{dp}{dx} = \frac{1}{6}\lambda_1\delta + \lambda_1 + 2\delta. \tag{A6}$$

As the core profile curvature, $\Gamma_1 = 0$, within the inlet region, and u_c and δ are given by Eqs. (A1) and (A5), λ_1 can easily be found through Eq. (A9). From which the axial pressure gradient can be found using the definition given in Eq. (A6). The pressure gradient found in this way can then be integrated over the axial coordinate X although the complex expressions involved require numerical integration. This procedure can be iterated until agreement between pressure drop agrees with the Bernoulli requirement ($\Delta p = u_c^2 - 1$)—i.e., using the velocity predicted by Eq. (A1) reaches agreement with the pressure drop found through the previous procedure to within 3% over the entire inlet region ($0.0007 < X < 0.036$).

2. Filled region

Within the filled region, the pressure gradient is somewhat different, given by

$$\lambda - 2\Gamma_1 \equiv \frac{\delta^2}{\mu u_c}\frac{dp}{dx} = \frac{1}{6}\lambda_1 + \lambda_1 + 2 - 2\Gamma_1. \tag{A7}$$

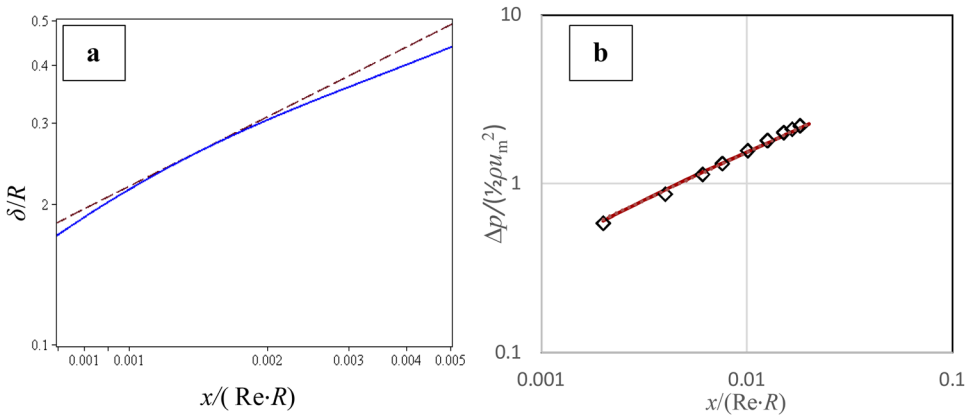

FIG. 15. Demonstration of the approximation's compliance with constraints: (a) the flat-plate boundary layer limit near the inlet and (b) self-consistency in pressure drop.

Therein, a new parameter has appeared—the velocity profile curvature at the axis, defined as

$$\Gamma_1 \equiv \frac{R^2}{u_c}\frac{\partial^2 u}{\partial r^2}\bigg|_{r=0} = -\frac{2}{7}\left(1-\exp\left(-\gamma_2\left(X-X_f\right)\right)\right). \tag{A8}$$

Here, the final value 2/7 emerges from introducing $\eta(r)$ into Eq. (1) and requiring convergence to the well-known parabolic profile. In addition, as this term comes into play in the filled region only beyond X_f, it is, therefore, approximated by the later exponential convergence, assuming that the normalized curvature develops in a similar way to the centerline velocity. Although, this assumption is not independently justified, it is shown to capture the flow well as a part of this approximate description.

For closure of the pressure drop description in the entire pipe, the final relation is given by

$$\lambda_1 = \frac{180-\left(24\delta^2-108\delta+9\Gamma_1+180\right)u_c}{u_c\delta(3-\delta)}. \tag{A9}$$

Thereby the use of this equation in conjunction with Eq. (A1) provides the pressure descriptions completed in each region—by Eqs. (A3) and (A6) for the inlet and by Eqs. (A7) and (A8) for the filled one.

In order to meet mass conservation, previous theory contains a singularity at the inlet—i.e., velocity and boundary layer begin to grow at an infinite rate. For the present approximation, limited to two exponential terms for centerline velocity, the initial gradient is large but finite. This means that mass conservation cannot be met at the inlet but rather is obtained to within 0.000 01% beyond a very short initial section—$X = 0.0007$ (not shown). This new approximation is further validated in the section titled Methods against previous data from the literature and against present numerical solutions.

REFERENCES

Abbas, M., Magaud, P., Gao, Y., and Geoffroy, S., "Migration of finite sized particles in a laminar square channel flow from low to high Reynolds numbers," Phys. Fluids **26**(12), 123301 (2014).

Andrade, E. N. C. and Tsien, L. C., "The velocity-distribution in a liquid-into-liquid jet," Phys. Soc. **49**(4), 381–391 (1937).

Bohr, N., "Determination of the surface-tension of water by method of jet vibration," Proc. R. Soc. Lond. A **82**(552), 146 (1909).

Davies, J. M., Hutton, J. F., and Walters, K., "A critical re-appraisal of the jet-thrust technique for normal stresses, with particular reference to axial velocity and stress rearrangement at the exit plane," J. Non-Newtonian Fluid Mech. **3**(2), 141–160 (1977).

Duda, J. L. and Vrentas, J. S., "Fluid mechanics of laminar liquid jets," Chem. Eng. Sci. **22**(6), 855–869 (1967).

Durst, F., Ray, S., Ünsal, B., and Bayoumi, O. A., "The development lengths of laminar pipe and channel flows," J. Fluids Eng. **127**(6), 1154 (2005).

Fargie, D. and Martin, B. W., "Developing laminar flow in a pipe of circular cross-section," Proc. R. Soc. London, Ser. A **321**, 461–476 (1971).

Friedmann, M., Gillis, J., and Liron, N., "Laminar flow in a pipe at low and moderate Reynolds numbers," Appl. Sci. Res. **19**(1), 426–438 (1968).

Gavis, J. and Modan, M., "Expansion and contraction of jets of Newtonian liquids in air: Effect of tube length," Phys. Fluids **10**(3), 487–497 (1967).

Greenshields, C. J., Weller, H. G., Gasparini, L., and Reese, J. M., "Implementation of semi-discrete, non-staggered central schemes in a colocated, polyhedral, finite volume framework, for high-speed viscous flows," Int. J. Numer. Methods Fluids **63**, 1–21 (2010).

Hashmi, S. M., Loewenberg, M., and Firoozabadi, A., "Colloidal asphaltene deposition in laminar pipe flow: Flow rate and parametric effects," Phys. Fluids **27**(8), 083302 (2015).

Haustein, H. D., Harnik, R. S., and Rohlfs, W., "A simple hydrodynamic model of a laminar free-surface jet in horizontal or vertical flight," Phys. Fluids **29**(8), 082105 (2017).

Hornbeck, R. W., "Laminar flow in the entrance region of a pipe," Appl. Sci. Res. **13**(1), 224–232 (1964).

Incropera, F. P., Bergman, T. L., Lavine, A. S., and Dewitt, D. P., *Fundamentals of Heat and Mass Transfer*, 7th ed. (John Wiley & Sons, 2011).

Kashi, B. and Haustein, D. H., "Dependence of submerged jet heat transfer on nozzle length," Int. J. Heat Mass Transfer **121**, 137 (2018).

Kashi, B. and Haustein, H. D., "Microscale sets a fundamental limit to heat transfer," Int. Commun. Heat Mass Transfer **104**, 1–7 (2019).

Kashi, B., Weinberg, E., and Haustein, H. D., "Analytical re-examination of the submerged laminar jet's velocity evolution," Phys. Fluids **30**, 063604 (2018).

Langhaar, H. L., "Steady flow in the transition length of a straight tube," J. Appl. Mech. **9**, 55–58 (1942).

Mamet, V., Namy, P., and Dedulle, J. M., "Numerical modeling of flow focusing: Quantitative characterization of the flow regimes," Phys. Fluids **29**(9), 093606 (2017).

Mohanty, A. K. and Asthana, S. B. L., "Imcompressible laminar and turbulent flow in the entrance region of a smooth circular pipe," in *6th Australian Hydraulics and Fluid Mechanics Conference* (The Institution of Engineers, Australia, 1977), pp. 5–9.

Mohanty, A. K. and Asthana, S. B. L., "Laminar flow in the entrance region of a smooth pipe," J. Fluid Mech. **90**(3), 433–447 (1979).

Priymak, V. G., "Direct numerical simulation of quasi-equilibrium turbulent puffs in pipe flow," Phys. Fluids **30**(6), 064102 (2018).

Reci, A., Sederman, A. J., and Gladden, L. F., "Experimental evidence of velocity profile inversion in developing laminar flow using magnetic resonance velocimetry," J. Fluid Mech. **851**, 545–557 (2018).

Revuelta, A., Sánchez, A. L., and Liñán, A., "The virtual origin as a first-order correction for the far-field description of laminar jets," Phys. Fluids **14**(6), 1821–1824 (2002).

Schiller, L., "Die enfwicklung der laminaren geschwindigkeitsverfeilung und ihre bedeufung fur zahigkeiismessungen," J. Appl. Math. Mech. **2**, 96–106 (1922).

Schlichting, H., "Laminare kanaleinlaufstromung," Zamm **14**, 368–373 (1934).

Schlichting, H., *Boundary Layer Theory*, 7th ed. (Mcgraw-Hill Book Company, 1967).

Schwarz, W. H. and Caswell, B., "Some heat transfer characteristics of the two-dimensional laminar incompressible wall jet," Chem. Eng. Sci. **16**, 338–351 (1961).

Shapiro, A. H., Siegel, R., and Kline, S. J., "Friction factor in the laminar entry region of a smooth tube," J. Appl. Mech. **21**(3), 289 (1954).

Sparrow, E. M., Lin, S. H., and Lundgren, T. S., "Flow development in the hydrodynamic entrance region of tubes and ducts," Phys. Fluids **7**(3), 338 (1964).

Stange, M., Dreyer, M. E., and Rath, H. J., "Capillary driven flow in circular cylindrical tubes," Phys. Fluids **15**(9), 2587–2601 (2003).

Suñol, F. and González-Cinca, R., "Liquid jet breakup and subsequent droplet dynamics under normal gravity and in microgravity conditions," Phys. Fluids **27**(7), 077102 (2015).

Umemura, A. and Osaka, J., "Self-destabilizing loop observed in a jetting-to-dripping transition," J. Fluid Mech. **752**, 184–218 (2014).

Watson, E. J., "The radial spread of a liquid jet over a horizontal plane," J. Fluid Mech. **20**(03), 481 (1964).